AMERICAN METEOROLOGICAL SOCIETY

Journal of Hydrometeorology

EARLY ONLINE RELEASE

The DOI for this manuscript is doi: 10.1175/JHM-D-14-0205.1

The final published version of this manuscript will replace the preliminary version at the above DOI once it is available.

If you would like to cite this EOR in a separate work, please use the following full citation:

Koster, R., and G. Walker, 2015: Interactive Vegetation Phenology, Soil Moisture, and Monthly Temperature Forecasts. J. Hydrometeor. doi:10.1175/JHM-D-14-0205.1, in press.

Interactive Vegetation Phenology, Soil Moisture, and Monthly Temperature Forecasts

R. D. Koster[1] and G. K. Walker[1,2]

[1]Global Modeling and Assimilation Office, NASA/GSFC, Greenbelt, MD

[2]SSAI, Lanham, MD

Corresponding author address:

Randal Koster

Global Modeling and Assimilation Office

Code 610.1, NASA/GSFC

Greenbelt, MD 20771

randal.d.koster@nasa.gov

Abstract

The time scales that characterize the variations of vegetation phenology are generally much longer than those that characterize atmospheric processes. The explicit modeling of phenological processes in an atmospheric forecast system thus has the potential to provide skill to subseasonal or seasonal forecasts. We examine this possibility here using a forecast system fitted with a dynamic vegetation phenology model. We perform three experiments, each consisting of 128 independent warm-season monthly forecasts: (1) an experiment in which both soil moisture states and carbon states (e.g., those determining leaf area index, or LAI) are initialized realistically; (2) an experiment in which the carbon states are prescribed to climatology throughout the forecasts; and (3) an experiment in which both the carbon and soil moisture states are prescribed to climatology throughout the forecasts. Evaluating the monthly forecasts of air temperature in each ensemble against observations – as well as quantifying the inherent predictability of temperature within each ensemble – shows that dynamic phenology can indeed contribute positively to subseasonal forecasts, though only to a small extent, with an impact dwarfed by that of soil moisture.

1. Introduction

The numerical models responsible for near-term weather forecasts (out to ~10 days) extract most of their forecast skill from the realistic representation of atmospheric conditions at the start of the forecast, as obtained through atmospheric analysis. The information content of atmospheric initial conditions, however, is soon dissipated by chaotic atmospheric dynamics, and thus forecasts at longer time scales must rely on connections with other, slower-moving components of the Earth system. Seasonal forecasts, for example, have long relied on models of the ocean circulation (e.g., Shukla, 1998). By coupling an ocean model to an atmospheric model, a predictable feature of the ocean circulation (or a predictable mode of the coupled ocean-atmosphere system) several months into a forecast can affect the atmosphere at this later time, potentially adding skill to the atmospheric forecast at that time. At subseasonal scales, soil moisture plays a similar role. The second phase of the Global Land-Atmosphere Coupling Experiment (GLACE-2; Koster et al. 2011) showed that an accurate initialization of soil moisture state can add significant skill to surface air temperature forecasts out to two months.

The "lushness" of vegetation (as represented by the leaf area index, or LAI) also has a persistence that exceeds that of atmospheric variables [Wang and Eltahir 2000, Zeng et al. 1999, Guillevic et al. 2002]. Because vegetation state has a direct impact on, for example, surface albedo and canopy transpiration conductance, models that include prognostic treatments of vegetation state – models that determine, in effect, variations in LAI in response to meteorological factors as well as the persistence of an LAI anomaly so induced – have, at least in theory, the potential to provide additional forecast skill at subseasonal or seasonal leads.

57 Such dynamic vegetation models, or DVMs, already exist and have been implemented
58 into the systems of many global climate modeling centers (e.g., Boussetta et al. 2013, Dunne et
59 al. 2013). These DVMs monitor the storage of carbon in various vegetation and soil reservoirs
60 and, in the process, provide estimates of the responses of vegetation phenology (e.g., LAI) to
61 variations in meteorological forcing. Their use to date, however, has generally not focused on
62 the meteorological prediction problem; mostly, they have been used in studies of the global
63 carbon cycle (e.g., Friedlingstein et al. 2014, Shao et al. 2014).

64 Indeed, very few studies have addressed the role of vegetation in meteorological
65 variability and prediction. Guillevic et al. (2002) quantified the impact of prescribed LAI
66 variability (i.e., from satellite-based observations rather than from a DVM) on the variability of
67 evapotranspiration and precipitation produced in an atmospheric general circulation model
68 (AGCM). Impacts on evapotranspiration were significant, but those on precipitation were
69 largely drowned out by atmospheric noise. Using a similar series of simulations, Weiss et al.
70 (2012) quantified the impact of LAI variability on the potential predictability in an AGCM, and
71 they also showed where the prescription of accurate LAI variations leads to reduced temperature
72 biases compared to observations. Bali (2014) followed the guidelines of the first Global Land-
73 Atmosphere Coupling Experiment (Koster et al. 2006) to determine coupling 'hot spots'
74 associated with variations in vegetation phenology. Weiss et al. (2014) used a fully interactive
75 DVM in an Earth system model to explore vegetation impacts on predictions at the decadal scale.

76 Given the availability of DVMs and the importance of predictions at all time scales, the
77 time is ripe for additional analyses. Here we focus on the subseasonal (in particular, monthly)
78 forecasting problem – we perform a series of forecast experiments with the National Aeronautics
79 and Space Administration Goddard Space Flight Center (NASA/GSFC) Earth modeling system

known as GEOS-5 (Global Earth Observing System, version 5), fitted with an explicit treatment of dynamic phenology. Our analysis focuses both on the idealized predictability associated with interactive phenology at subseasonal timescales and on the actual forecast skill contributed by the use of realistically initialized interactive phenology, as determined by comparing forecasted quantities with observations.

The system used and the experiments performed are discussed in Section 2. Results for predictability and forecast skill are presented in Sections 3, with additional discussion provided in Section 4.

2. Framework for Analysis

a. Modeling System

The Global Modeling and Assimilation Office of NASA GSFC hosts GEOS-5, a state-of-the-art Earth system model (Molod et al. 2012). In its complete form, the GEOS-5 modeling system consists of coupled atmosphere, ocean, land, and sea-ice models. When run with full data assimilation machinery, GEOS-5 has produced, among other things, a well-utilized climate reanalysis (Rienecker et al. 2011). Data assimilation is also used to initialize the coupled models for seasonal forecasts of precipitation and temperature; the GEOS-5 seasonal forecasts are accessible on the web (http://gmao.gsfc.nasa.gov/cgi-bin/products/climateforecasts/GEOS5/index.cgi) and contribute to the North American Multi-Model Analysis (Kirtman et al. 2014).

In this study we utilize the land and atmosphere components of the GEOS-5 system, prescribing persisted sea surface temperature (SST) and sea ice anomalies through each 1-month forecast period. As with other models of its kind, the GEOS-5 atmospheric model supplements its treatment of atmospheric dynamics with parameterizations of unresolvable physical processes. For example, it treats convection with the Relaxed Arakawa-Schubert parameterization scheme (Moorthi and Suarez 1992), and it treats prognostic cloud cover using the techniques of Bacmeister et al. (2006), accounting for such processes as the auto-conversion and accretion of cloud water particles and the re-evaporation of falling precipitation. It treats longwave and shortwave radiation processes (with absorption from various chemical and aerosol species) as described by Chou and Suarez (1994) and Chou (1990, 1992), respectively. Turbulence near the surface is parameterized according to Lock (2000). The surface layer parameterization used is based on the Monin-Obukhov approach described by Helfand and Schubert (1995). We modified the surface layer parameterization so that it includes a viscous sublayer over land; the default application of the parameterization applies the viscous sublayer only over non-land surfaces.

The Catchment land surface model (Koster et al. 2000), the model standardly used within operational GEOS-5 systems, performs a complete energy and water budget calculation at every time step, accounting for such processes as canopy interception, vegetation resistance to transpiration, and runoff production through both baseflow and overland flow. The model treats statistically the subgrid-scale spatial variability of soil moisture known to exist in nature – at each time step, the areal fractions of the surface element existing in different hydrological regimes are computed from the model's soil moisture prognostic variables and from a statistical

description of the topography within the element. Different, regime-specific treatments of evaporation and runoff production are applied within the different areal fractions.

Again, the present forecasting study is unique in its consideration of dynamic vegetation phenology at the land surface. The Catchment land surface model was recently enhanced through the inclusion of the prognostic carbon (and thus prognostic phenology) elements of the National Center for Atmospheric Research - Department of Energy (NCAR/DOE) Community Land Model version 4 (CLM4) DVM (Oleson et al. 2010). The CLM4 DVM's photosynthesis physics produces, as a matter of course, an estimate of canopy transpiration conductance that is consistent with its calculation of carbon uptake. This conductance is provided to the Catchment model, which uses it to update the surface energy and water budgets. Koster et al. (2014) describe how the models were combined and highlight some unique features of the merged Catchment-CN model, including its ability to represent multiple, hydrological regime-specific vegetation states within a surface element.

Koster et al. (2014) also analyze offline simulations (i.e., uncoupled from the atmosphere) performed with this model. Their comparisons of simulated FPAR (fraction of absorbed photosynthetically active radiation, a key indicator of phenology) with satellite-based estimates from the GIMMS dataset (Tucker et al. 2005) demonstrate that the merged model, while biased, does capture well the key controls of water supply on vegetation behavior. The Catchment-CN model was shown in the study to be a useful tool for the analysis of climate-vegetation connections.

b. Experiments Performed

144 Using the GEOS-5 system (with a grid resolution of 2.5º longitude × 2º latitude), we
145 perform three forecast experiments, also summarized briefly in Table 1:

146 Experiment OA: "Ocean-Atmosphere". Initial atmospheric and ocean conditions
147 differ between forecasts, whereas soil moisture and vegetation prognostic
148 variables are maintained at (seasonally-varying) climatological values determined
149 for the period 1979-2010 from the offline simulation discussed below.

150 Experiment OAW: "Ocean-Atmosphere-Soil Moisture". Same as Experiment
151 OA, but with soil moisture no longer prescribed, and with its initial conditions set
152 to observations-based values.

153 Experiment OAWV: "Ocean-Atmosphere-Soil Moisture-Vegetation". Same as
154 experiment OA, but with both soil moisture and vegetation state no longer
155 prescribed, and with both sets of initial conditions set to observations-based
156 values.

157 Each experiment consists of 128 independent monthly forecasts, four (initialized on May 1, June
158 1, July 1, and August 1) for each year of the period 1979-2010. Each forecast in turn consists of
159 21 ensemble members, generated through slight perturbations of the atmospheric initial
160 conditions. For all forecasts, atmospheric initial conditions were extracted for the given start
161 date from an independent free-running AGCM simulation, and the prescribed SST and sea ice
162 distributions consist of observed SST and sea ice anomalies for the start date (derived from
163 http://www-pcmdi.llnl.gov/projects/amip/AMIP2EXPDSN/BCS/amip2bcs.php) added to
164 corresponding climatological seasonal cycles.

The soil moisture initial conditions for Experiments OAW and OAWV and the vegetation initial conditions for Experiment OAWV were extracted from an offline simulation with the Catchment-CN model covering the period 1948-2010, performed following the approach outlined in Koster et al. (2014). Because this offline simulation utilized observations-based meteorological forcing (Sheffield et al. 2006), the soil moisture and carbon states produced and then used for forecast initialization are arguably realistic, with, for example, high soil moisture and possibly high LAI following extended rainy periods. As a result, these initial moisture and vegetation states can potentially contribute skill to the monthly forecasts.

We quantify here the contributions of soil moisture and vegetation to predictability and forecast skill by differencing the results of the different experiments. The contributions of soil moisture are isolated by differencing the results of Experiments OAW and OA; likewise, the contributions of vegetation state are isolated by differencing the results of Experiments OAWV and OAW.

c. Observations Used for Forecast Evaluation

Forecast skill evaluations are made against monthly 2-m air temperature values produced by the ERA-Interim reanalysis (Dee et al. 2011). To ensure a clean comparison, the reanalysis fields were regridded to the 2.5°× 2° resolution used by our forecast system.

3. Results

a. Predictability

Predictability is a fundamental property of nature and of a modeling system (National Research Council, 2010). In essence, it describes how long the effects of an initial state are felt in the climate system before the "memory" of that state is erased by chaotic dynamics. Predictability for a modeling system is typically characterized by examining how the spread amongst the ensemble members of a forecast increases with time. While such predictability is an intrinsic property of the model and is necessarily model-dependent, the hope is that it reflects the (unmeasurable) predictability that exists in nature; in any case, it provides one upper limit for the forecast skill attainable with that particular forecast system.

We compute predictability here as follows. First, every ensemble member of every forecast is standardized into a Z-score (i.e., forecasted values are converted to anomalies divided by standard deviation) so that forecasts for different months can be considered together. The first ensemble member of each forecast is then considered the "truth" against which the ensemble mean of the remaining ensemble members is tested – an established procedure in predictability calculations (e.g., Becker et al. 2014). We compute the square of the correlation coefficient (r^2) between the "truth" simulation results and the ensemble mean results. We then repeat the process taking the second ensemble member in each forecast as the "truth", and so on. The average of the 21 r^2 values so computed is our measure of predictability. This average can range from 0, implying that the initial conditions have no impact whatsoever on the forecast, to 1, implying that they completely determine the forecast.

The results for 2-m air temperature are shown in Figure 1. Figure 1a shows high predictability over the oceans in Experiment OA, certainly a reflection of the prescribed interannually-varying SSTs. These SSTs are presumably also responsible for the high

predictability levels over tropical land (Koster et al. 2000), whereas the smaller but still significant values over midlatitude land probably stem in part from the atmospheric initialization.

Figure 1b shows the equivalent map for Experiment OAW, and more importantly, Figure 1c shows the difference between Figures 1b and 1a, i.e., the contribution of soil moisture initialization and dynamics to surface air temperature predictability. The contributions are high over many midlatitude land areas, particularly in the transition zones between dry and wet areas – places where the evaporation is both reasonably high and sensitive to soil moisture variations (Koster et al. 2000).

Indeed, Figure 1c is comparable to the predictability map presented by Koster et al. (2011), with similar patterns over all continents except perhaps Australia. (Perfect agreement would not be expected in any case, since the patterns in Koster et al. [2011] represent a multi-model estimate of predictability.) Figure 1c is presented here mainly as context for Figure 1e, the difference between Figures 1d and 1b. Figure 1e offers the isolated contribution of initialized vegetation state and subsequent interactive vegetation phenology to surface air temperature predictability. While this contribution is substantially smaller than that for soil moisture, it is still generally positive, particularly equatorward of about 45°. Low contributions are seen in the deserts, where vegetation is always sparse, and in lushly vegetated tropical areas, where presumably variations in phenology do not limit transpiration – atmospheric demand (energy availability) is known to limit total evapotranspiration in the lush tropics (e.g., Koster et al. 2000), so variations in the leafiness of the trees should have minimal impact there. The negative values seen in higher latitudes presumably reflect sampling error; results for individual months (not shown) indicate that negative high-latitude differences are by far the largest in May and June, when snow may still be present and vegetation may not have a large impact.

231 Importantly, the pattern seen in Figure 1e agrees strongly with patterns of interannual
232 vegetation variability known to exist in the model (see Figure 7c of Koster et al. [2014]). The
233 spatial correlation of the pattern in Figure 1e with that of the average monthly standard deviation
234 of FPAR produced in Experiment OAWV (an indication of where we would expect vegetation to
235 have an effect) over all non-ice land points is 0.35, which far exceeds the 99.99% confidence
236 level. Such pattern agreement gives us confidence that the differences seen in Figure 1e reflect
237 true vegetation contributions to predictability, even if many of the values seen in the figure are
238 too small to pass a significance test when examined in isolation.

239 Figure 2a shows, as a function of forecast month, the estimated predictability
240 contributions from soil moisture and phenology averaged over land. Interactive phenology is
241 seen to contribute the most in July and August, but in every month its contribution is much lower
242 than that of interactive soil moisture. The final two histogram bars show the contributions when
243 all months are considered together (i.e., the global land averages of the differences shown in
244 Figures 1c and 1e). Phenology contributes an average of about 0.004 to the total predictability,
245 which is much smaller than the corresponding value (0.024) from soil moisture.

246

247 **b. Forecast Skill**

248 Predictability, while important to quantify, is not as tangible as forecast skill. Our
249 experimental design allows us to quantify the contributions of both soil moisture
250 initialization/dynamics (as in GLACE-2 [Koster et al. 2011]) and vegetation
251 initialization/dynamics to the skill of surface air temperature forecasts through a comparison of
252 the forecasts with observations.

253 Such skill, however, must not be evaluated everywhere. In regions with poorly estimated
254 precipitation, the land surface conditions produced by our offline Catchment-CN simulation will
255 themselves be poor. The forecast initializations in these regions therefore cannot be trusted, and
256 neither can the locally forecasted 2-m air temperatures. We mask out these regions in our
257 forecast evaluation using the map of rain gauge density in Figure 3, which was derived from data
258 at http://www.esrl.noaa.gov/psd/data/gridded/data.precl.html. This density map is relevant, for
259 example, to the construction of the Global Precipitation Climatology Project product, which
260 underlies the Sheffield et al. (2006) forcing dataset used in our offline simulation. In essence,
261 any $2.5^{o} \times 2^{o}$ grid cell containing less than one precipitation gauge on average over the period
262 1979-2010 is not considered in our forecast evaluation.

263 The spatial distributions of intrinsic model predictability associated with soil moisture
264 and vegetation should also be considered. If a region shows a negligible contribution of
265 predictability from either soil moisture or vegetation in Figure 1, any skill (negative or positive)
266 in the region seemingly derived from the land variable must in fact reflect sampling error and is
267 not real. We therefore apply a second mask to the forecast skill results based on the
268 predictability contributions shown in Figure 1c,e. We do not consider skill contributions from
269 soil moisture if the predictability associated with soil moisture is below 0.005. Similarly, we do
270 not show skill contributions from vegetation phenology if the predictability contributions from
271 phenology lie below 0.005.

272 With these masks in place, we present in Figure 4a the contribution of soil moisture
273 initialization and subsequent dynamics to skill in the 1-month forecast of 2-m air temperature,
274 where skill is measured as the square of the correlation coefficient (r^2) between the standardized
275 observations and the standardized ensemble means of the forecasts. In analogy to Figure 1c, soil

moisture contributions to skill are obtained by subtracting the skill levels of Experiment OA from those of Experiment OAW. Much of the world in Figure 4a is indeed masked out; our ability to evaluate skill is limited. North America, however, does host a continental-scale region with both adequate rain gauge density and inherent contributions to predictability from soil moisture, and here, large contributions to forecast skill, up to 0.1, are seen in a swath extending from the southern Great Plains toward the northwest. Other regions with significant skill contributions include the Nordeste region of Brazil and the eastern part of southern Africa. Negative skill contributions do show up in various areas, indicating that sampling error is still an issue despite the masks applied. The positive values, however, show field significance, far outweighing the negative values.

Figure 4b shows the corresponding contributions from phenology initialization and dynamics, obtained by subtracting the skill levels in Experiment OAW from those of experiment OAWV. Phenology contributions to skill are clearly smaller than those of soil moisture, but they still appear mostly positive across the globe. Contributions in the southwest United States, for example, are as high as 0.05. Regions of positive skill contributions are also seen in Nordeste, southern Africa, and northeastern China.

The global averages of the skill contributions from soil moisture and phenology are compared in Figure 2b. For the averaging, only the rain gauge density mask is applied so that both sets of skill contributions are averaged over the same land areas. Average phenology contributions to skill are small but positive in every month; in August, the contribution rivals that of soil moisture. (Of course, locally the phenology contributions can be much higher than indicated in the histogram – see Figure 4b.) The spatial correlation between the increase in skill levels (for the combined months) and the average monthly standard deviation of simulated FPAR

299 in the unmasked areas of Figure 4b is 0.45, which is significant at the 99.99% level and thus
300 indicative of a true impact of vegetation phenology initialization and dynamics on skill.

301

302 **4. Discussion**

303 The results above show that initializing vegetation phenology at the start of a monthly
304 forecast and allowing it to interact with the climate system during the forecast leads to a small
305 increase in monthly temperature forecast skill in certain locations – a contribution dwarfed by
306 that of soil moisture and yet still promisingly important, given the current state-of-the-art in
307 monthly forecasting. Corresponding analysis (not shown) suggests that phenology contributes
308 no significant skill to the forecasts of monthly precipitation.

309 Caveats to the analysis are, of course, worth noting. First, the design of the forecasts was
310 not ideal in every way – the atmosphere, for example, was not initialized with fields from a
311 reanalysis, and SST anomalies were persisted rather than predicted using a coupled ocean model.
312 Arguably, though, the experimental framework makes these particular issues secondary.
313 Because we isolate soil moisture and phenology contributions by subtracting the results of
314 different experiments, the atmospheric and ocean contributions to skill (presumably the same in
315 the experiments) effectively cancel out.

316 Presumably more limiting are inherent deficiencies in the models used and in the soil
317 moisture and carbon initializations applied. Like all models, the Catchment-CN land surface
318 model has its biases (Koster et al. 2014), and the data used to initialize the model are based on
319 biased measurements. The question that must be asked in all modeling studies is how
320 experimental results and associated scientific conclusions are affected by these biases. It seems

reasonable to assume that any biases that do exist would only hamper the model's ability to take advantage of soil moisture and phenology initialization and dynamics. That is, we can reasonably assume that the forecast skill contributions shown in Figures 2b and 4 are lower bounds for the skill that would be achieved with a perfect system. How much the skill levels could still increase is unknown, though one upper bound for the current modeling system, under perfect initialization data, is effectively provided by the predictability levels shown in Figure 1.

Prospects for improving the initialization of the soil moisture and carbon reservoirs (and thus LAI) rest largely with the development of data assimilation systems that combine, through a modeling framework, observations-based meteorological forcing data with satellite-based estimates of soil moisture and vegetation state (e.g., Reichle et al. 2007). New soil moisture estimates from L-band sensors (Kerr et al. 2010, Entekhabi et al. 2010) show particular promise for assimilation efforts, and estimates of FPAR (fraction of absorbed photosynthetically active radiation), as derived from NDVI (normalized difference vegetation index) through established techniques (e.g. Sellers et al. 1996), can also theoretically be assimilated, given the existence of FPAR-related variables in DVMs. A substantial amount of satellite-based soil moisture and vegetation data does indeed exist (or will soon exist) but remains currently untapped for the subseasonal forecasting problem.

We close with a final note about the role of dynamic phenology in forecast systems. We have been careful not to imply that the phenology-related skill contributions in Figure 4b stem only from the initialization of the carbon states underlying the phenology, for they could also stem from the interaction of the phenology with the rest of the climate system during the forecast period. This is a subtle yet important point. Even if phenology is not initialized accurately, the fact that the phenology can interact with soil moisture during the forecast period, so that

phenological variations can move in concert with soil moisture variations during the period, may provide skill to a forecast beyond what can be derived from soil moisture alone. In other words, interactive phenology, regardless of its own initialized state, may be able to amplify the impact of a realistic soil moisture initialization for the better. More work is needed to address this particular idea, but preliminary analyses (not shown here) do suggest that the idea has merit.

5. Summary

The experiments described above isolate the impact of dynamic vegetation phenology – its initialization and subsequent prognostic treatment – on the monthly air temperatures generated in a forecast system. Phenology is seen to contribute to both the predictability of 2-m air temperature (Figures 1e, 2a) and the skill of air temperature forecasts (Figures 2b, 3b). The contributions are not large and are indeed dwarfed by those of soil moisture, which are also quantified and are presented for context. Nevertheless, the inclusion of dynamic phenology does have a positive impact on the forecast system.

Again, the study is naturally limited by deficiencies in the modeling system used and in the data underlying its initialization. Addressing these deficiencies would presumably only increase the ability of phenology initialization and dynamics to contribute to skill. We consider the extraction of some phenology-related skill, even in light of existing limitations, to be an encouraging result.

Acknowledgments. We thank Peter Thornton for his help with the development of the Catchment-CN model. This research was supported by NASA's Modeling, Analysis, and Prediction Program.

References

Bacmeister, J. T., M. J. Suarez, and F. R. Robertson, 2006: Rain reevaporation, boundary layer convection interactions, and Pacific rainfall patterns in a AGCM. J.Atmos. Sci., 63, 3383-3403.

Bali, M., 2014: Land-atmosphere coupling strength in ECHAM5/JSBACH model. Climate Dynamics, under review.

Becker, E., H. van den Dool, and Q. Zhang, 2014: Predictability and forecast skill in NMME. J. Climate, 27, 5891-5906.

Boussetta, S., and Coauthors, 2013: Natural land carbon dioxide exchanges in the ECMWF integrated forecasting system: Implementation and offline validation. J. Geophys. Res. Atmos., 118, 5923–5946, doi:10.1002/jgrd.50488.

Chou, M.-D., 1992: A solar radiation model for use in climate studies. J. Atmos. Sci., 49, 762-772.

Chou, M.-D., 1990: Parameterizations for the absorption of solar radiation by O2 and CO2 with applications to climate studies. J. Climate, 3, 209-217.

Chou, M. -D., and M.J. Suarez, 1994: An efficient thermal infrared radiation parameterization for use in general circulation models, NASA Tech. Memorandum 104606-Vol 3, NASA, Goddard Space Flight Center, Greenbelt, MD.

Dee, D. P., and Co-authors, 2011: The ERA-Interim reanalysis: configuration and performance of the data assimilation system. Q. J. Royal Met. Soc., 137, 553-597.

388 Dunne, J. P., and Coauthors, 2013: GFDL's ESM2 global coupled climate–carbon Earth system
389 models. Part II: Carbon system formulation and baseline simulation characteristics. *J.*
390 *Climate*, **26**, 2247–2267, doi:10.1175/JCLI-D-12-00150.1.

391 Entekhabi, D., and Co-authors, 2010: The Soil Moisture Active Passive (SMAP) mission. Proc.
392 IEEE, 98, 704-716.

393 Friedlingstein, P., M Meinshausen, V. K. Arora, C. D. Jones, A. Anav, S. K. Liddicoat, and R.
394 Knutti, 2014: Uncertainties in CMIP5 climate projections due to carbon cycle feedbacks.
395 J. Climate, 27, 511-526.

396 Guillevic, P., R. D. Koster, M. J. Suarez, G. J. Collatz, L. Bounoua, and S. O. Los, 2002:
397 Influence of vegetation interannual variability on hydrological processes over land
398 surfaces. *J. Hydrometeorology*, **3**, 617-629.

399 Helfand, H. M., M. and S. D. Schubert, 1995: Climatology of the Simulated Great Plains Low-
400 Level Jet and Its contribution to the Continental Moisture Budget of the United States. J.
401 Climate, 8, 784-806.

402 Kerr, Y. H., and Co-authors, 2010: The SMOS mission: New tool for monitoring key elements of
403 the global water cycle. Proc. IEEE, 98, doi:10.1109/JPROC.2010.2043032.

404 Kirtman, B. P., and Co-authors, 2014: The North American multi-model ensemble. *Bull. Amer.*
405 *Met. Soc.*, **95**, 585-601, 2014.

406 Koster, R. D., M. J. Suarez, A. Ducharne, M. Stieglitz, and P. Kumar, 2000: A catchment-based
407 approach to modeling land surface processes in a general circulation model: 1. Model
408 structure, *J. Geophys. Res.*, **105**(20), 24,809– 24,822.

Koster, R. D., M. J. Suarez, and M. Heiser, 2000: Variance and predictability of precipitation at seasonal-to-interannual timescales. *J. Hydromet*., **1**, 26-46.

Koster, R. D., and Coauthors, 2006: GLACE: TheGlobal Land–Atmosphere Coupling Experiment. Part I: Overview. J. Hydrometeor., 7, 590–610.

Koster, R. D., and Co-authors, 2011: The second phase of the Global Land-Atmosphere Coupling Experiment, Soil moisture contributions to subseasonal forecast skill. J. Hydromet., 12, 805-822.

Koster, R. D., G. K. Walker, G. J. Collatz, and P. E. Thornton, 2014: Hydroclimatic controls on the means and variability of vegetation phenology and carbon uptake. J. Climate, 27, 5632-5652.

Lock, A. P., A. R. Brown, M. R. Bush, G. M. Martin, and R. N. B. Smith, 2000: A new boundary layer mixing scheme. Part I: Scheme description and single-column model tests. Mon. Wea. Rev., 138, 31873199.

Molod, A., L. Takacs, M. Suarez, J. Bacmeister, I.-S. Song, and A. Eichmann, 2012: The GEOS-5 atmospheric general circulation model, Mean climate and development from MERRA to Fortuna. Tech. Rep. Ser. on Global Modeling and Data Assimilation, 28, NASA/TM-2012-104606, 115 pp.

Moorthi, S., and M. J. Suarez, 1992: Relaxed Arakawa Schubert: A parameterization of moist convection for general circulation models. Mon. Wea. Rev., 120, 978-1002.

National Research Council, 2010: Assessment of intraseasonal to interannual climate prediction and predictability. The National Academies Press, Washington, D.C, 181 pp.

Oleson, K. W., and Co-authors, 2010: Technical description of version 4.0 of the Community Land Model (CLM). NCAR Technical Note NCAR/TN-478+STR., National Center for Atmospheric Research, P. O. Box 3000, Boulder, Colorado, 80307-3000.

Reichle, R. H., R. D. Koster, P. Liu, S. P. P. Mahanama, E. G. Njoku, and M. Owe, 2007: Comparison and assimilation of global soil moisture retrievals from the Advanced Microwave Scanning Radiometer for the Earth Observing System (AMSR-E) and the Scanning Multichannel Microwave Radiometer (SMMR). J. Geophys. Res., 112, D09108, doi:10.1029/2006JD008033.

Rienecker, M. M., and Co-Authors, 2011: MERRA, NASA's Modern-Era Retrospective Analysis for Research and Applications. *J. Climate*, **24**, 3624-3648.

Sellers, P. J., S. O. Los, C. J. Tucker, C. O. Justice, D. A. Dazlich, G. J. Collatz, and D. A. Randall, 1996: A revised land surface parameterization (SiB2) for atmospheric GCMs, Part II, The generation of global fields of terrestrial biophysical parameters from satellite data. J. Climate, 9, 706-737.

Shao, P., X. Zeng, K. Sakaguchi, R. K. Monson, and X. Zeng, 2014: Terrestrial carbon cycle, Climate relations in eight CMIP5 Earth system models. J. Climate, 26, 8744-8764.

Sheffield, J., G. Goteti, and E. F. Wood, 2006: Development of a 50-year high-resolution global dataset of meteorological forcings for land surface modeling. J. Climate, 19, 3088-3111.

Shukla, J., 1998: Predictability in the midst of chaos, A scientific basis for climate forecasting. Science, 282, 728-731.

Tucker, C. J., and Co-authors, 2005: An extended AVHRR 8-km NDVI dataset compatible with MODIS and SPOT vegetation NDVI data. Int. J. Rem. Sens., 26, 4485-4498.

Wang, G., and E. A. B. Eltahir, 2000: Role of vegetation dynamics in enhancing the low-frequency variability of the Sahel rainfall. Water Resour. Res., 36, 1013-1021.

Weiss, M., B. van den Hurk, R. Haarsma, and W. Hazeleger, 2012: Impact of vegetation variability on potential predictability and sill of EC-Earth simulations. Clim. Dyn., 39, 2733-2746.

Weiss, M., P. Miller, B. van den Hurk, T. van Noije, S. , R. Haarsma, L. van Ulft, W. Hazeleger, P. Le Sager, B. Smith, and G. Schurgers, 2014: Contribution of dynamic vegetation phenology to decadal climate predictability. J. Climate, 27, 8563-8577, doi:10.1175/JCLI-D-13-00684.1.

Zeng, N., J. D. Neelin, K.-M. Lau, and C. J. Tucker, 1999: Enhancement of interdecadal climate variability in the Sahel by vegetation interaction. Science, 286, 1537-1540.

Table 1. Summary of Forecast Experiments.

Forecast Experiment Identifier	Soil Moisture Treatment	Vegetation Phenology Treatment
OA	Climatological	Climatological
OAW	Initialized realistically; prognostically followed	Climatological
OAWV	Initialized realistically; prognostically followed	Initialized realistically; prognostically followed

Figure Captions

Figure 1. a. Surface air temperature predictability as generated in Experiment OA. (See text for details of the calculation.) b. Same, but for Experiment OAW. c. Differences between the fields in (b) and (a), effectively showing the contribution of soil moisture initialization and dynamics to air temperature predictability. d. Same as (a), but for Experiment OAWV. e. Same as (c), but for the difference between the fields in (d) and (b), effectively showing the contribution of vegetation initialization and dynamics to air temperature predictability.

Figure 2. Top: Soil moisture (blue) and vegetation (green) contributions to air temperature predictability for each month individually and for all four months considered together, averaged over all land points (excluding Greenland and Antarctica). Bottom: Same, but for air temperature forecast skill, and averaged over all non-ice land points with a rain gauge density exceeding 1 gauge per 2°×2.5° grid cell.

Figure 3. Average rain gauge density (number of gauges per 2°×2.5° grid cell) underlying the PREC/L and GPCP monthly rainfall products during 1979-2010.

Figure 4. a. Contribution of soil moisture initialization and dynamics to air temperature forecast skill. Two masks are applied – results are shown only for: (i) grid cells with a rain gauge density greater than 1 gauge per 2°×2.5° grid cell, and (ii) grid cells for which the predictability associated with soil moisture initialization is greater than 0.005 (see Figure 1c). b. Same, but for the contribution of vegetation initialization and dynamics to air

503 temperature forecast skill, and with the predictability contribution mask derived from
504 Figure 1e.

505

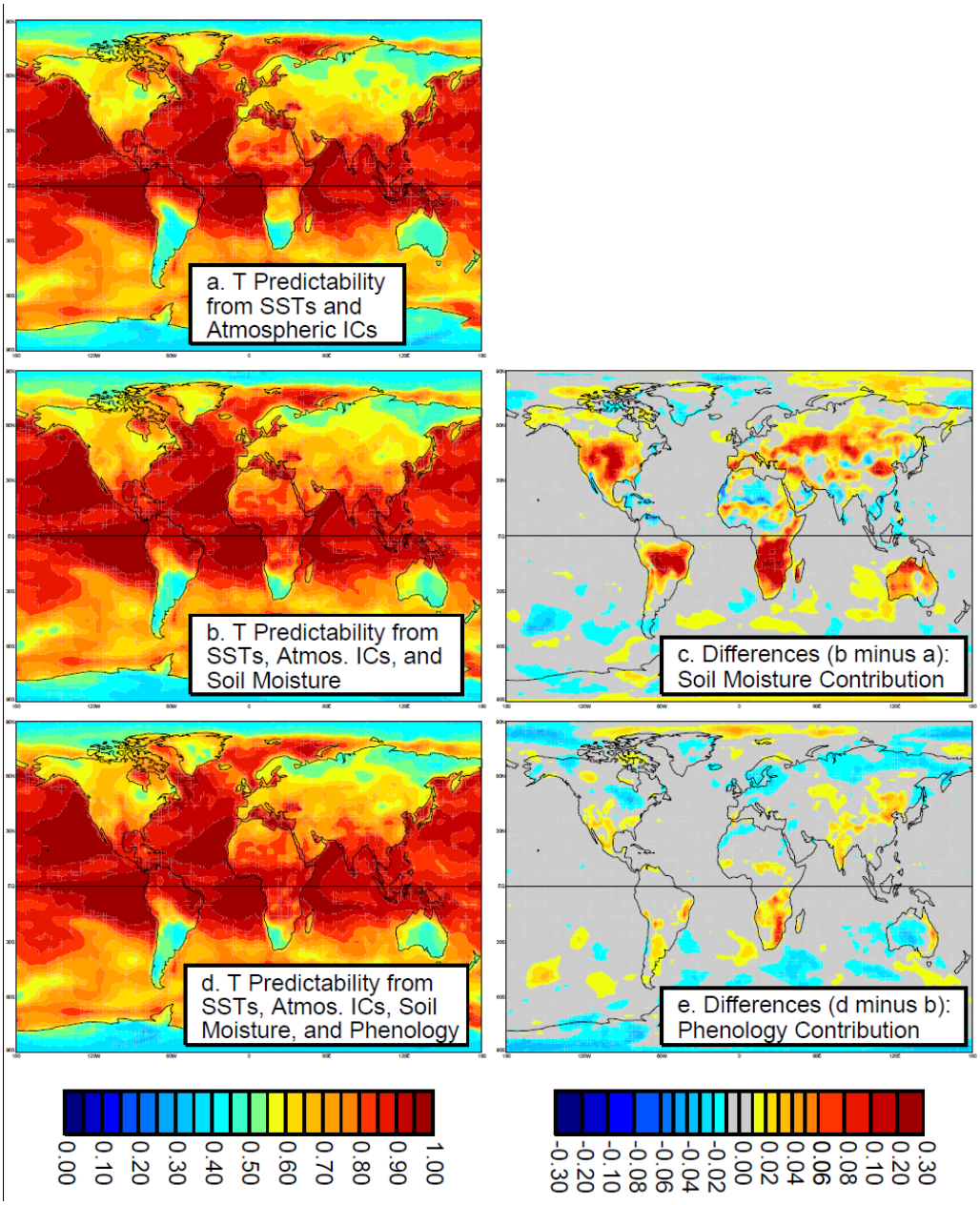

Figure 1. a. Surface air temperature predictability as generated in Experiment OA. (See text for details of the calculation.) b. Same, but for Experiment OAW. c. Differences between the fields in (b) and (a), effectively showing the contribution of soil moisture initialization and dynamics to air temperature predictability. d. Same as (a), but for Experiment OAWV. e. Same as (c), but for the difference between the fields in (d) and (b), effectively showing the contribution of vegetation initialization and dynamics to air temperature predictability.

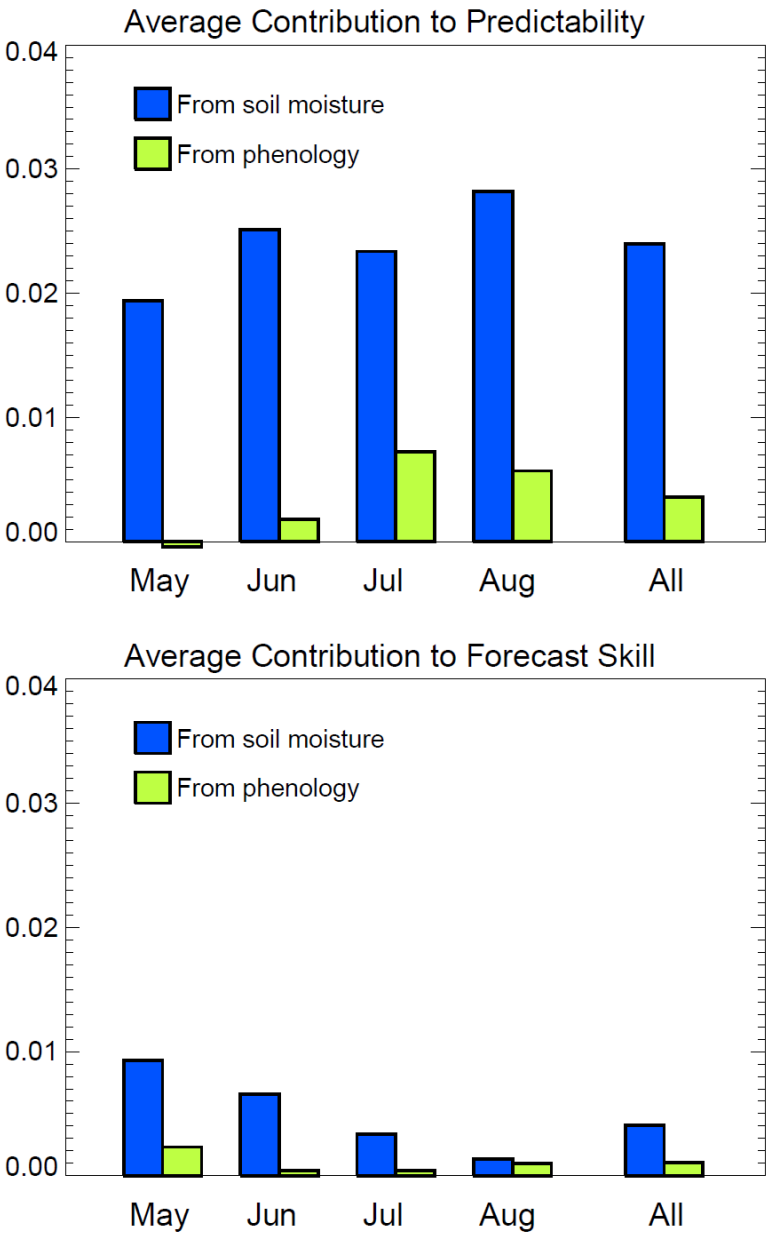

Figure 2. Top: Soil moisture (blue) and vegetation (green) contributions to air temperature predictability for each month individually and for all four months considered together, averaged over all land points (excluding Greenland and Antarctica). Bottom: Same, but for air temperature forecast skill, and averaged over all non-ice land points with a rain gauge density exceeding 1 gauge per 2°×2.5° grid cell.

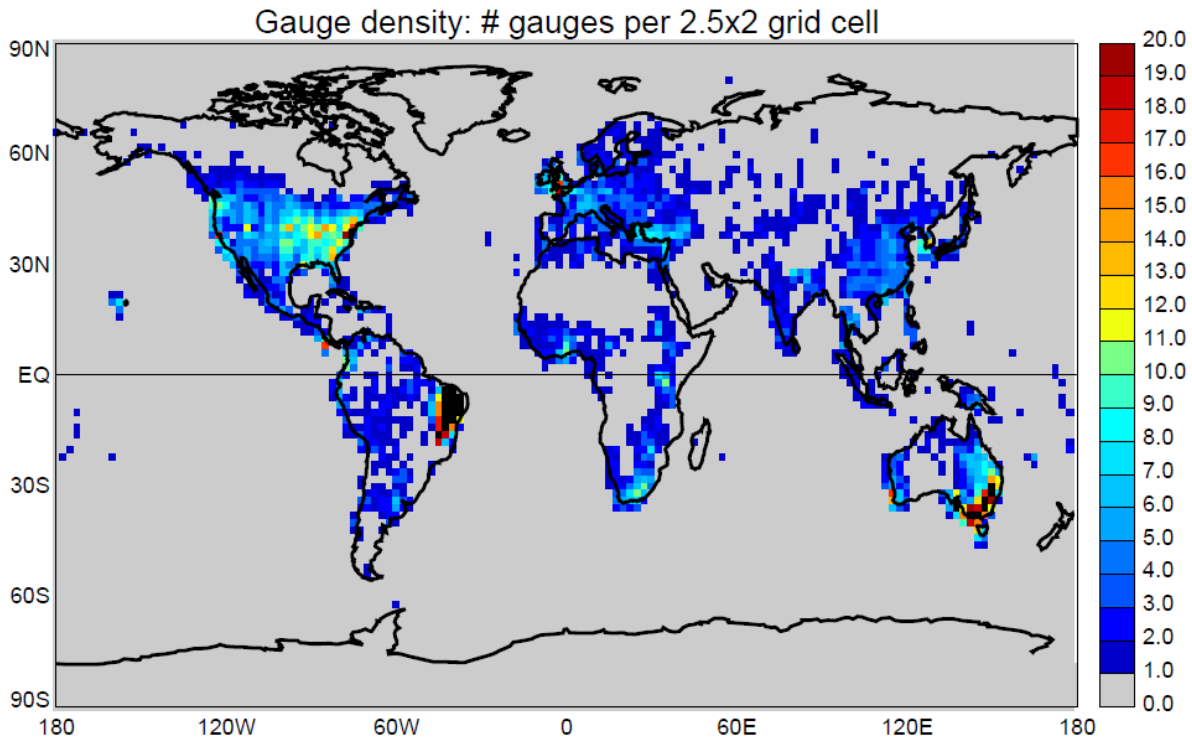

Figure 3. Average rain gauge density (number of gauges per 2°×2.5° grid cell) underlying the PREC/L and GPCP monthly rainfall products during 1979-2010.

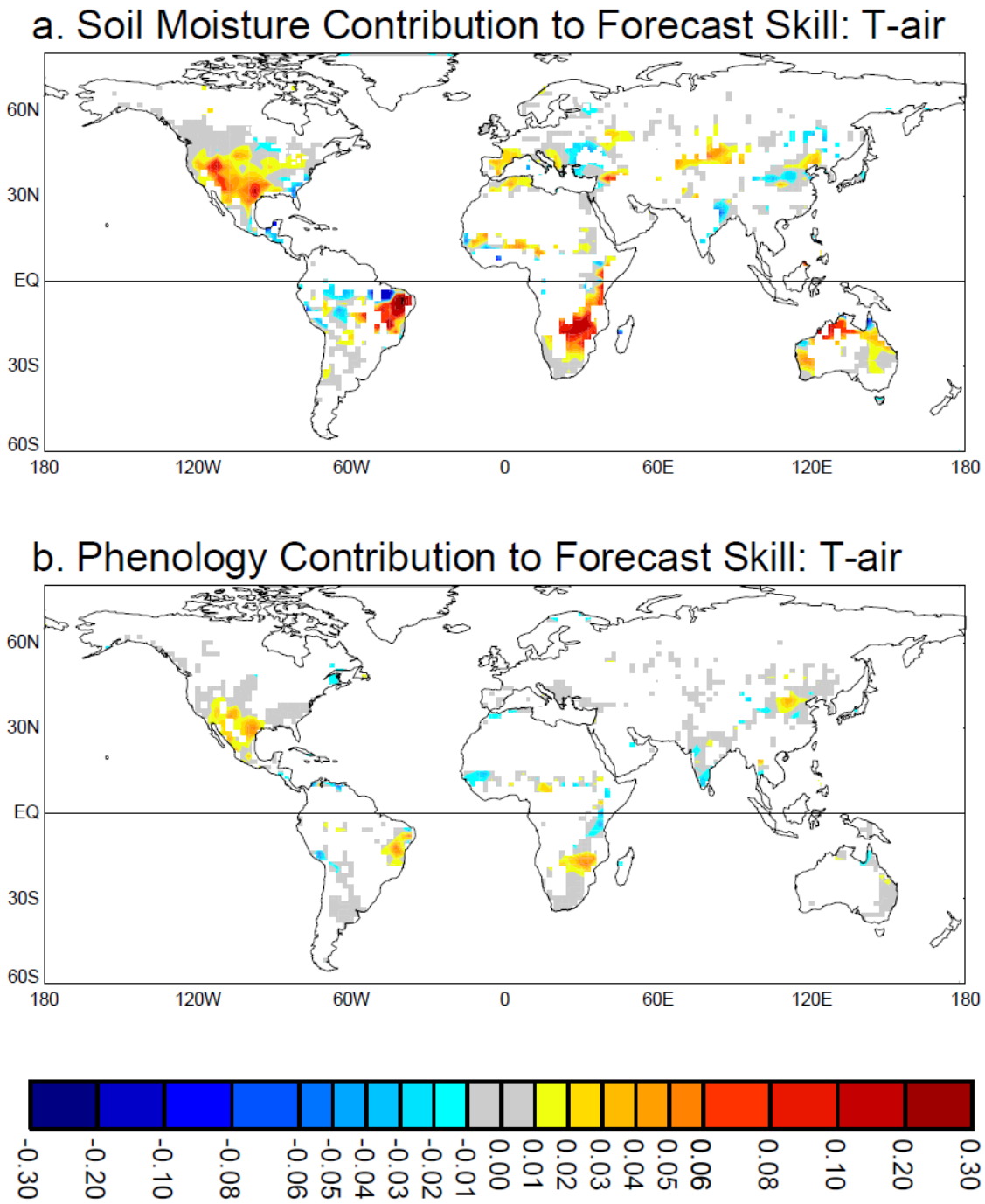

Figure 4. a. Contribution of soil moisture initialization and dynamics to air temperature forecast skill. Two masks are applied – results are shown only for: (i) grid cells with a rain gauge density greater than 1 gauge per 2°×2.5° grid cell, and (ii) grid cells for which the predictability associated with soil moisture initialization is greater than 0.005 (see Figure 1c). b. Same, but for the contribution of vegetation initialization and dynamics to air temperature forecast skill, and with the predictability contribution mask derived from Figure 1e.